PLOS ONE

RESEARCH ARTICLE

# Spontaneous low frequency BOLD signal variations from resting-state fMRI are decreased in Alzheimer disease

**Samaneh Kazemifar[1,2☯], Kathryn Y. Manning[1,2‡], Nagalingam Rajakumar[3‡], Francisco A. Gómez[4‡], Andrea Soddu[5‡], Michael J. Borrie[6,7‡], Ravi S. Menon[1,2☯], Robert Bartha[1,2☯*], for the Alzheimer's Disease Neuroimaging Initiative[¶]**

**1** Centre for Functional and Metabolic Mapping, Robarts Research Institute, University of Western Ontario, London, Ontario, Canada, **2** Department of Medical Biophysics, University of Western Ontario, London, Ontario, Canada, **3** Department of Anatomy and Cell Biology, University of Western Ontario, London, Ontario, Canada, **4** Department of Mathematics, Universidad Nacional de Colombia, Sede Bogotá, Colombia, **5** Department of Physics and Astronomy, University of Western Ontario, London, Ontario, Canada, **6** Department of Medicine, University of Western Ontario, London, Ontario, Canada, **7** Division of Aging, Rehabilitation and Geriatric Care, Lawson Health Research Institute, London, Ontario, Canada

☯ These authors contributed equally to this work.
‡ These authors also contributed equally to this work.
¶ Membership of the Alzheimer's Disease Neuroimaging Initiative is provided in the Acknowledgments.
* rbartha@robarts.ca





**Citation:** Kazemifar S, Manning KY, Rajakumar N, Gómez FA, Soddu A, Borrie MJ, et al. (2017) Spontaneous low frequency BOLD signal variations from resting-state fMRI are decreased in Alzheimer disease. PLoS ONE 12(6): e0178529. https://doi.org/10.1371/journal.pone.0178529

**Editor:** Kewei Chen, Banner Alzheimer's Institute, UNITED STATES

**Received:** January 2, 2017

**Accepted:** May 15, 2017

**Published:** June 5, 2017



**Data Availability Statement:** We obtained all data for this manuscript from a third party: the Alzheimer's Disease Neuroimaging Initiative. The data are available to all researchers using an online application that can be found at the following website: http://adni.loni.usc.edu/datasamples/access-data/. In the revised manuscript, we have included a listing of all subject ID numbers and scan dates (S1 and S2 Tables) used in the current manuscript. These ID numbers can be used to identify the data used in the current study within the ADNI database. We would appreciate your

## Abstract

Previous studies have demonstrated altered brain activity in Alzheimer's disease using task based functional MRI (fMRI), network based resting-state fMRI, and glucose metabolism from $^{18}$F fluorodeoxyglucose-PET (FDG-PET). Our goal was to define a novel indicator of neuronal activity based on a first-order textural feature of the resting state functional MRI (RS-fMRI) signal. Furthermore, we examined the association between this neuronal activity metric and glucose metabolism from $^{18}$F FDG-PET. We studied 15 normal elderly controls (NEC) and 15 probable Alzheimer disease (AD) subjects from the AD Neuroimaging Initiative. An independent component analysis was applied to the RS-fMRI, followed by template matching to identify neuronal components (NC). A regional brain activity measurement was constructed based on the variation of the RS-fMRI signal of these NC. The standardized glucose uptake values of several brain regions relative to the cerebellum (SUVR) were measured from partial volume corrected FDG-PET images. Comparing the AD and NEC groups, the mean brain activity metric was significantly lower in the accumbens, while the glucose SUVR was significantly lower in the amygdala and hippocampus. The RS-fMRI brain activity metric was positively correlated with cognitive measures and amyloid $\beta_{1-42}$ cerebral spinal fluid levels; however, these did not remain significant following Bonferroni correction. There was a significant linear correlation between the brain activity metric and the glucose SUVR measurements. This proof of concept study demonstrates that this novel and easy to implement RS-fMRI brain activity metric can differentiate a group of healthy elderly controls from a group of people with AD.

advice on any further information that is needed regarding data accessibility.

**Funding:** This study was funded by the Canadian Institute of Health Research (www.cihr-irsc.gc.ca/) with grant CSE 133350. Data collection and sharing for this project was funded by the Alzheimer's Disease Neuroimaging Initiative (National Institutes of Health Grant U01 AG024904) and DOD ADNI (Department of Defense award number W81XWH-12-2-0012). ADNI is funded by the National Institute on Aging, the National Institute of Biomedical Imaging and Bioengineering, and through generous contributions from the following: AbbVie, Alzheimer's Association; Alzheimer's Drug Discovery Foundation; Araclon Biotech; BioClinica, Inc.; Biogen; Bristol-Myers Squibb Company; CereSpir, Inc.; Eisai Inc.; Elan Pharmaceuticals, Inc.; Eli Lilly and Company; EuroImmun; F. Hoffmann-La Roche Ltd and its affiliated company Genentech, Inc.; Fujirebio; GE Healthcare; IXICO Ltd.; Janssen Alzheimer Immunotherapy Research & Development, LLC.; Johnson & Johnson Pharmaceutical Research & Development LLC.; Lumosity; Lundbeck; Merck & Co., Inc.; Meso Scale Diagnostics, LLC.; NeuroRx Research; Neurotrack Technologies; Novartis Pharmaceuticals Corporation; Pfizer Inc.; Piramal Imaging; Servier; Takeda Pharmaceutical Company; and Transition Therapeutics. The Canadian Institutes of Health Research is providing funds to support ADNI clinical sites in Canada. Private sector contributions are facilitated by the Foundation for the National Institutes of Health (www.fnih.org). The grantee organization is the Northern California Institute for Research and Education, and the study is coordinated by the Alzheimer's Disease Cooperative Study at the University of California, San Diego. ADNI data are disseminated by the Laboratory for Neuro Imaging at the University of Southern California. The funders had no role in study design, data collection and analysis, decision to publish, or preparation of the manuscript.

**Competing interests:** ADNI is funded by the National Institute on Aging, the National Institute of Biomedical Imaging and Bioengineering, and through generous contributions from the following: AbbVie, Alzheimer's Association; Alzheimer's Drug Discovery Foundation; Araclon Biotech; BioClinica, Inc.; Biogen; Bristol-Myers Squibb Company; CereSpir, Inc.; Eisai Inc.; Elan Pharmaceuticals, Inc.; Eli Lilly and Company; EuroImmun; F. Hoffmann-La Roche Ltd and its affiliated company Genentech, Inc.; Fujirebio; GE Healthcare; IXICO Ltd.; Janssen Alzheimer Immunotherapy Research & Development, LLC.; Johnson & Johnson

## Introduction

Alzheimer disease is considered to be a progressive neurodegenerative condition clinically characterized by cognitive dysfunction and memory impairments [1] that appear to result from the pathological accumulation of amyloid plaques and neurofibrillary tangles [2, 3]. Brain atrophy measured by magnetic resonance imaging (MRI) has been established as an important biomarker associated with disease progression and treatment response [4–6]. Another established biomarker is reduced regional uptake of $^{18}$F labeled fluorodeoxyglucose (FDG) measured using positron emission tomography (PET) [7], indicating lower glucose metabolism in Alzheimer's disease [8, 9].

Neuronal activity can also be inferred from blood oxygen level dependent (BOLD) contrast as exploited in functional MRI (fMRI). More recently, resting state fMRI (RS-fMRI) measures of spontaneous low frequency fluctuations ($< 0.1$ HZ) in the BOLD signal have been used to identify functionally connected brain regions (networks) without the performance of an overt task [10, 11]. Previous studies [12, 13] have shown that several resting state networks can be identified, and may be altered in Alzheimer's disease. For example, multiple studies have found RS-fMRI can be used to show disrupted connectivity between the hippocampus and other brain regions in Alzheimer disease [13–15]. Furthermore, the interconnectivity of brain regions can be used to classify subjects with Alzheimer disease, amnestic mild cognitive impairment, and healthy elderly [16].

A number of different statistical and mathematic approaches have been used to infer functional connectivity from RS-fMRI data. One common approach is to use the *a-priori* selection of a seed region of interest (ROI) [17–19] to determine the correlation between the mean BOLD signal time course within the ROI and the BOLD signal time courses of all other pixels in the brain. However the requirement for *a-priori* seed selection makes it difficult to examine the functional connectivity across the whole brain. Another popular multivariate technique for analyzing whole brain connectivity is independent component analysis (ICA) [20–22]. This approach does not require *a-priori* information and decomposes the BOLD signal into a set of spatial and temporal components that are maximally statistically independent [23]. The ICA method is also an efficient approach to extract scanner noise, as well as physiological and motion artifacts from the BOLD signal [24]. One of the major challenges with the ICA technique is to determine which components represent physiologically relevant networks, and which components represent noise. However methods now exist to differentiate neuronal from non-neuronal components [25].

Brain regions associated with the default mode network (DMN) have been repeatedly implicated in the pathogenesis of Alzheimer's disease [13, 26]. FDG-PET studies have shown reduced glucose metabolism in the medial temporal cortex, hippocampus, and posterior cingulate cortex [27–29]. Decreased functional connectivity in the DMN has also been associated with increased amyloid deposition measured using Pittsburgh compound B PET [30, 31]. In addition, several studies in healthy controls have shown a relationship between glucose metabolism measured by PET and the RS-fMRI signal. For example, Di *et. al.* showed that metabolic activity was correlated with independent component (IC) maps of the BOLD signal in regions that are functionally connected [32]. Similarly, Tomasi *et. al.* [33] measured the amplitude of the RS-fMRI signal and glucose metabolism by FDG-PET and demonstrated that higher metabolism was correlated with a higher amplitude of the RS-fMRI signal in the cerebellum, occipital, and parietal cortices. Finally, Riedl *et. al.* [34] found a correlation between local brain activity in specific regions of interest measured from FDG-PET data and functional connectivity measured by RS-fMRI using seed-based methods.

Pharmaceutical Research & Development LLC.; Lumosity; Lundbeck; Merck & Co., Inc.; Meso Scale Diagnostics, LLC.; NeuroRx Research; Neurotrack Technologies; Novartis Pharmaceuticals Corporation; Pfizer Inc.; Piramal Imaging; Servier; Takeda Pharmaceutical Company; and Transition Therapeutics. The Canadian Institutes of Health Research is providing funds to support ADNI clinical sites in Canada. Private sector contributions are facilitated by the Foundation for the National Institutes of Health (www.fnih.org). The partial funding of the ADNI by industry does not alter our adherence to PLOS ONE policies on sharing data and materials.

Previous RS-fMRI studies have shown a reduction in functional connectivity between structures based on the *strength* of the correlation in the BOLD signal [18, 35]. Here, we define a novel metric of brain activity based on a first-order texture feature defined as the standard deviation of the *magnitude* of the BOLD fluctuation. The purpose of this study was to determine whether this new metric could be used to accurately differentiate healthy elderly individuals from people with mild Alzheimer disease. Our hypothesis was that the fluctuation of the magnitude of the BOLD signal as a function of time is related to neuronal activity and therefore will also correlate with FDG-PET measures of glucose metabolism. Our goal was to demonstrate the efficacy of a new indicator of Alzheimer's disease based on the fluctuation of the magnitude of the RS-fMRI signal. Furthermore, we examined the association between the fluctuation magnitude of the neuronal derived RS-fMRI signal and FDG-PET.

## Theory

In this study, we propose a brain activity measurement derived directly from the RS-fMRI signal. The RS-fMRI signal can be represented as an $i$ x $v$ matrix, where $i$ represents each pixel, and $v$ represents the number of volumes acquired in the fMRI acquisition. The ICA method decomposes the RS-fMRI signal into: 1) an $i$ x $n$ matrix of independent component spatial maps, where $n$ represents the number of components, and 2) an $n$ x $v$ matrix of mixing weights ($W$) or IC time-courses. Here, the number ($k$) of legitimate ICs was identified using a goodness-of-fit (GoF) calculation, a multiple template matching method and a support vector machine (SVM) classifier [25] that included only the neuronal components ($NC$) (Fig 1A). The weighting function for each neuronal component, $W_k(t_v)$ is then multiplied (Hadamard product, Eq 1, Fig 1B) with the equal length vector given by the RS-fMRI time series for each pixel, $S_i(t_v)$, generating a new vector of equal length $BSA_{i,k}(t_v)$:

$$BSA_{i,k}(t_v) = S_i(t_v) \circ W_k(t_v) \quad (1)$$

where $BSA_{i,k}$ represents the BOLD signal *amplitude* ($BSA$) for each neuronal component $k$ in pixel $i$. Then, the standard deviation (SD) is calculated for $BSA_{i,k}$ and is multiplied with the neuronal component ($NC_{i,k}$) (Fig 1C). The sum of this metric (Eq 2, Fig 1D) for all neuronal components in a pixel represents the neuronal activity and is used to produce a neuronal activity map.

$$Neuronal\ Activity_i = \sum_{j=1}^{k} \sqrt{SD(BSA_{i,j}(t_v)) \times NC_{i,j}} \quad (2)$$

## Materials and methods

### Study subjects

Data used in the preparation of this article (S1 and S2 Tables) were obtained from the Alzheimer's Disease Neuroimaging Initiative (ADNI) database (adni.loni.usc.edu). The ADNI was launched in 2003 as a public-private partnership, led by Principal Investigator Michael W. Weiner, MD. The primary goal of ADNI has been to test whether serial magnetic resonance imaging, positron emission tomography, other biological markers, and clinical and neuropsychological assessment can be combined to measure the progression of mild cognitive impairment and early Alzheimer's disease. Written informed consent for participation in the study was obtained from each participant, or their family. Data acquisition was approved by the local ethics review board at each participating site.

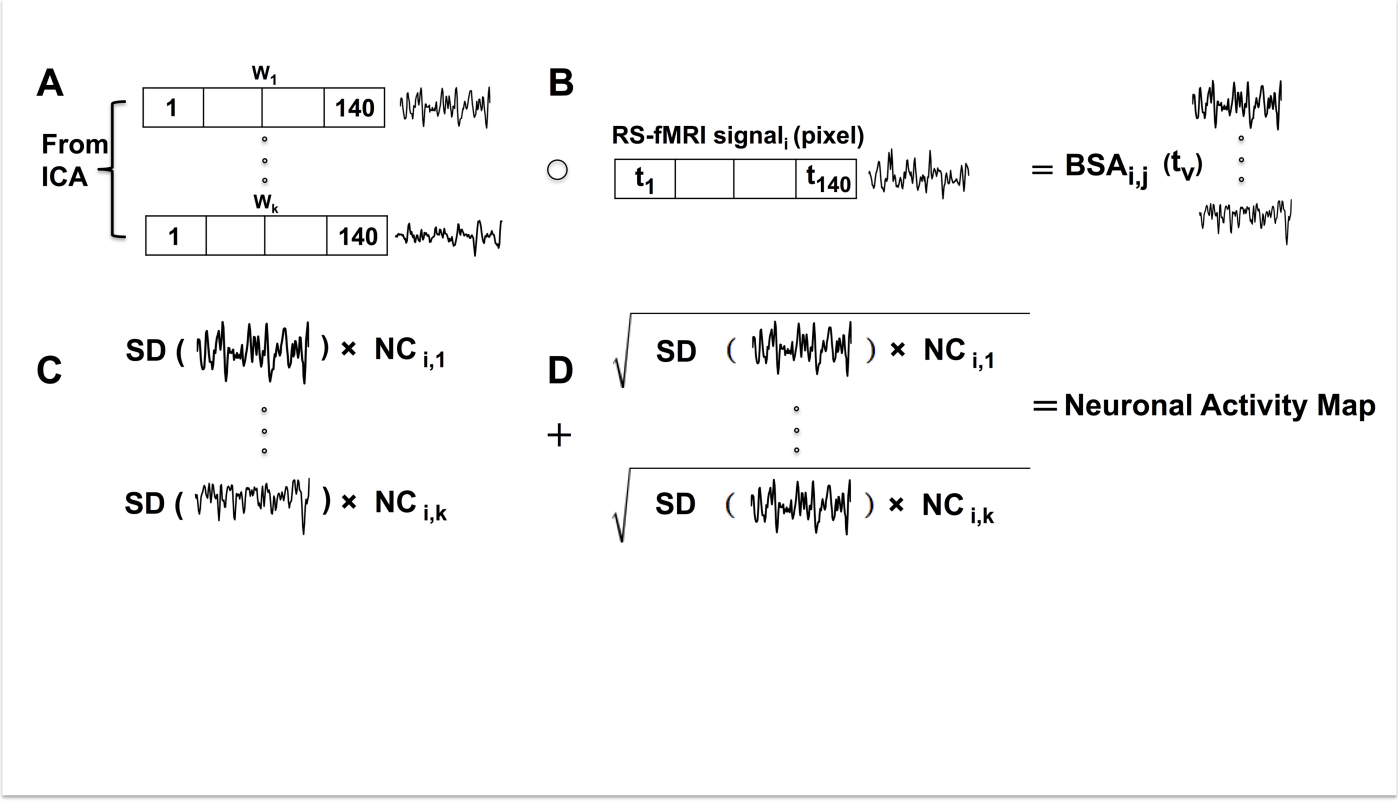


**Fig 1. Schematic diagram of the brain activity metric calculated from the RS-fMRI signal in one pixel.** The signal shown is a graphical representation of the vector data. (A) Neuronal time courses (*W*) are defined by the ICA and verified using a goodness of fit calculation, multiple template matching method and a support vector machine classifier. (B) The Hadamard product of each neuronal time course is taken with the RS-fMRI signal. (C) The standard deviation of the resulting signal is multiplied by the neuronal component. (D) The square root of the contribution of each neuronal time course is added to create a measure of neuronal activity.

https://doi.org/10.1371/journal.pone.0178529.g001

To test the algorithm, this study included data from 15 normal elderly controls (NEC) and 15 subjects with probable Alzheimer disease of mild severity obtained from the ADNI database. We included participants that had 3.0 Tesla $T_1$-weighted anatomical scans and 10-minute RS-fMRI data acquisitions. A subset of this group (13 NEC, and 11 subjects with mild Alzheimer disease) also had an FDG-PET scan available. Structural $T_1$-weighted images were obtained using a sagittal 3D magnetization-prepared rapid acquisition with a gradient echo MP-RAGE sequence with pixel size 1mm×1mm×1.2mm; flip angle ~9˚; TE ~4 ms; TR ~7 ms; matrix, 256x256; 170 slices [36]. The RS-fMRI scans were acquired using a single shot echo planer imaging (EPI) pulse sequence with pixel size 3.3mm×3.3mm×3.3mm; flip angle 80.0˚; TE 30 ms; TR ~3000 ms; matrix = 64x64; 48 slices [37]. FDG-PET images were acquired using similar protocols on all PET scanners but varied somewhat in resolution, spacing, and dimension. However images were normalized and motion corrected [38] prior to analysis. The FDG-PET scans consisted of six-5 minute frames acquired starting 30 minutes after FDG injection [38]. All frames were registered to the first frame and then averaged to produce a single static image. All subjects were also evaluated with the mini mental state examination (MMSE) [39] to assess cognition. In addition, CSF biomarkers including total Tau protein (Tau), phosphorylated Tau protein (P-Tau) and amyloid-β ($A\beta_{1-42}$) were obtained for all subjects (https://ida.loni.usc.edu/).

## RS-fMRI analysis

The brain was extracted from the RS-fMRI data and the anatomical $T_1$-weighted images using the brain extraction tool (BET) in the FSL software (functional MRI of the brain (FMRIB) Software Library, Department of Clinical Neurosciences, University of Oxford, UK, http://fsl.fmrib.ox.ac.uk/fsl/fslwiki/FSL). The brain extracted fMRI data were preprocessed, aligned and co-registered to the MNI-152 space using the fMRI expert analysis tool (FEAT) in FSL. An initial smoothing (full-width half-maximum of 6 mm), and band-pass temporal filtering (0.01 Hz —0.1 Hz) were applied before ICA decomposition. The ICA method (30 components) was performed using the group ICA of the fMRI toolbox (GIFT) [40]. The ICA was followed by a previously described three-step process [25] to identify neuronal components in each RS-fMRI data set, all implemented in-house by Demertzi and *et. al.* [25]. First, a goodness of fit (GoF) calculation was used to measure the similarity value between a component and established resting state networks [25]. Second, the multiple templates matching method was applied. Then, a template had to be assigned to one of the 30 components [25]. Thirdly, a support vector machine was used to label each component as neuronal, non-neuronal, or undefined [25].

Following identification of the neuronal components, a brain activity map was constructed from these components as described in the Theory section and co-registered to the MNI-152 standard image using linear and non-linear registration methods. Co-registration of the brain activity map to the anatomical image was conducted using Statistical Parametric Mapping (SPM8, Wellcome Department of Neurology, London, UK; www.fil.ion.ucl.ac.uk/spm). ROIs were defined in the MNI-152 image using the structural segmentation method called FMRIB's integrated registration and segmentation tool (FIRST) in FSL because it is easily accessible to the research community and automated. Finally, the mean intensity from each ROI in the brain activity map was measured. A schematic representation of the steps involved in making the brain activity measurements is provided in Fig 2.

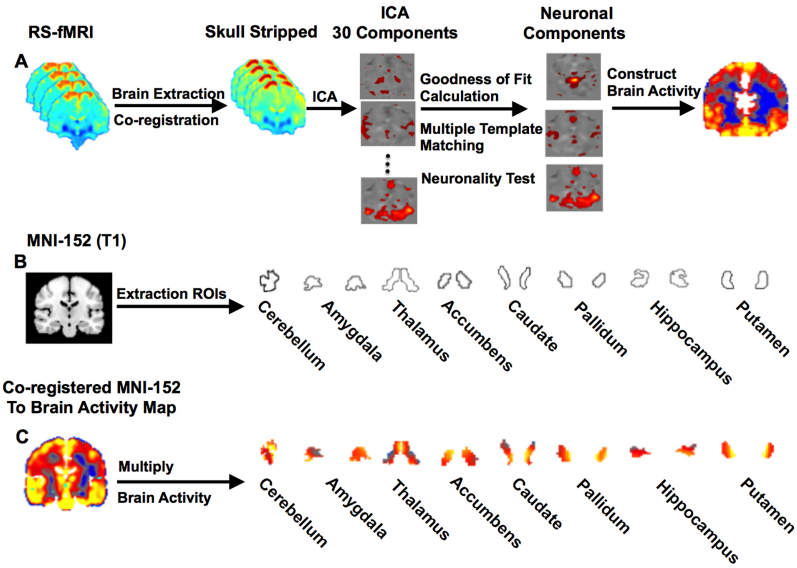


**Fig 2. Brain activity from RS-fMRI.** Schematic diagram of the brain activity (BOLD signal amplitude) measurement in different brain regions. (A) Steps involved in calculating the brain activity maps from the RS-fMRI. (B) Regions of interest extracted from MNI-152 space. (C) Activity maps within each region of interest from one subject.

https://doi.org/10.1371/journal.pone.0178529.g002

## Volumetric analysis

The FSL software was used to measure the volumes of the accumbens, amygdala, hippocampus, caudate nucleus, thalamus, pallidum, putamen, and whole brain from the $T_1$-weighted image of each subject using a method similar to that previously described [41]. The volumes were normalized to the whole brain volume in each subject.

## FDG-PET analysis

The brain was also extracted from the FDG-PET images using the BET tool in FSL. A partial volume correction method was applied to each data set using the partial volume correction structural functional synergistic resolution recovery (PVC_SFSRR) software [42]. This software performs pre-processing steps including co-registration of the FDG-PET with the structural image, segmentation and smoothing (8 mm), and finally partial volume correction. The corrected FDG-PET image was co-registered to the MNI-152 template. The predefined ROIs in the MNI-152 image were applied to the co-registered FDG-PET image. The standardized uptake value (SUV) of each ROI was then normalized to the mean SUV of the cerebellum to obtain the SUV ratio (SUVR) as this has been previously shown [43] to be unchanged in healthy subjects and at the early stages of Alzheimer disease.

## Statistical analysis

Prism GraphPad (Prism, version 6.00; GraphPad Software, San Diego, CA) and Matlab toolbox (version R2010a) were used for the statistical analyses. One-way ANOVA was used to compare brain activity between the NEC and Alzheimer disease groups ($p< 0.05$ considered significant). If a significant group effect was observed, the $p$-values associated with follow-up group comparisons between brain regions were Bonferroni corrected for multiple comparisons. The association between the brain activity measured from the RS-fMRI, MMSE score, and CSF biomarkers were evaluated using linear regression. The significance of these associations was Bonferroni corrected for multiple comparisons. The Pearson correlation coefficient was used to measure the association between the brain activity in gray matter obtained from RS-fMRI and the glucose uptake from FDG-PET ($p < 0.05$ considered significant).

## Classification model

To determine if the RS-fMRI derived brain activity measurement was a suitable biomarker to differentiate patients with mild Alzheimer disease and healthy elderly controls, a SVM classifier was used. Specifically, a linear SVM [44] was trained and tested on the feature space. Regions of interest were selected based on the observed differences between groups for either the brain activity metric or FDG-PET measured glucose metabolism. A leave-one-out-test was used as a cross-validation to predict the label for each test subject (not involved in the training phase). The accuracy, sensitivity, and specificity were determined after each subject was assessed as the test subject. In the first analysis, RS-fMRI brain activity in the hippocampus and accumbens, FDG-PET in the hippocampus, and hippocampal volume were evaluated separately. In a second analysis, FDG-PET and RS-fMRI modalities were evaluated independently incorporating data from both the hippocampus and amygdala. In a third analysis, we combined the volumetric and RS-fMRI information from the hippocampus and accumbens.

**Table 1. Demographic information for study participants.**

| | RS-fMRI NEC | RS-fMRI Alzheimer disease | FDG-PET NEC | FDG-PET Alzheimer disease |
|---|---|---|---|---|
| Number of subject (N) | 15 | 15 | 13 | 11 |
| Age (years) (Mean±SD) | 73.5 ± 6.2 | 73.3 ±8.0 | 74.4 ± 6.1 | 70.9 ± 7.2 |
| MMSE (Mean±SD) | 28.9 ± 1.2 | 21.6 ± 2.1* | 29.0 ± 1.1 | 21.8± 2.3* |
| Sex (F) | 10 | 10 | 9 | 7 |
| Tau (pg/ml) (Mean±SEM) | 66.3± 9.8 | 164.5±22.8** | 63.8±9.6 | 182.5±28.2** |
| P-Tau (pg/ml) (Mean±SEM) | 38.9 ± 10.0 | 62.0±7.7 | 40.7±11.1 | 68.1±9.5 |
| $A\beta_{1-42}$ (pg/ml) (Mean±SEM) | 192.5± 16.1 | 132.3±5.4** | 179.0±15.0 | 131.2±7.3** |

* $p < 0.05$ (two-tailed) and

** adjusted $p$ value (Bonferroni) between NEC and Alzheimer disease within a single imaging modality

F = female; SEM = standard error of mean, SD = standard deviation, NEC = normal elderly controls, FDG-PET = $^{18}$fludeoxyglucose-PET, RS-fMRI = resting state functional MRI, MMSE = mini mental state examination, P-Tau = phospho-Tau, $A\beta_{1-42}$ = amyloid $beta_{1-42}$.

https://doi.org/10.1371/journal.pone.0178529.t001

## Results

### Brain maps of neuronal activity and glucose metabolism

Demographic characteristics are provided in Table 1 for all 30 subjects (S1 and S2 Tables). There was no difference between group mean ages (healthy elderly subjects age range: 65–80 years; subjects with Alzheimer disease age range: 63–79 years), however as expected, there was a significant difference in the MMSE score ($p < 0.0001$, two-tailed t-test) between the two groups. Montreal neurological institute-152 (MNI-152) template $T_1$-weighted images (Fig 3A and 3B)

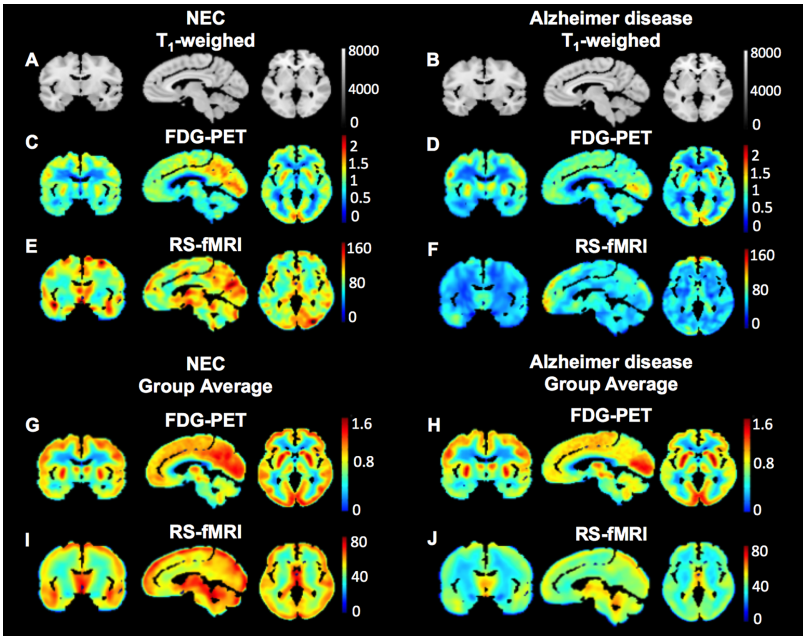


**Fig 3. Brain activity and glucose metabolism maps.** MNI-152 $T_1$-weighted anatomical images in coronal, sagittal, and axial orientations (A, B). Corresponding FDG-PET SUVR images of glucose metabolism from a healthy elderly subject, and healthy elderly group averaged (C, G); a patient with Alzheimer disease, and Alzheimer disease group averaged (D, H). Brain activity maps obtained using RS-fMRI in the same healthy elderly subject, and healthy elderly group averaged (E, I) and patient with Alzheimer disease, and Alzheimer disease group averaged (F, J).

https://doi.org/10.1371/journal.pone.0178529.g003

in coronal, sagittal, and axial planes are shown with corresponding standardized uptake value ratio (SUVR) glucose metabolism maps from the FDG-PET scan in one healthy elderly subject (Fig 3C) and the healthy elderly group average (Fig 3G); as well as one subject with Alzheimer disease (Fig 3D) and the Alzheimer disease group average (Fig 3H). Corresponding brain activity maps measured from the RS-fMRI in the same subjects (Fig 3E and 3F) and group averages (Fig 3I and 3J) are also provided. There is a visible decrease in signal in the subject with Alzheimer disease throughout the brain measured by both modalities.

## Comparison of regional brain activity and glucose metabolism

The average brain activity measured from RS-fMRI (Fig 4) is shown for the cerebellum, amygdala, thalamus, accumbens, caudate, pallidum, hippocampus, and putamen regions for the NEC and Alzheimer disease groups. Similarly, the average relative rate of glucose metabolism (Fig 5) is provided for the same regions measured by FDG-PET for the NEC and Alzheimer disease groups. A one-way ANOVA indicated that there was a significant difference between the two groups in RS-fMRI brain activity ($p<0.0001$) and FDG-PET measured glucose metabolism ($p<0.0001$). In follow-up comparisons, the difference in brain activity measured by RS-fMRI in both sides of the accumbens (adjusted $p = 0.04$) and differences in relative glucose metabolism measured using FDG-PET in the amygdala (adjusted $p = 0.02$), and hippocampus (adjusted $p = 0.006$) remained significant following Bonferroni correction. A one-way ANOVA indicated that there was also a significant difference between these groups in the Tau, P-Tau and $A\beta_{1-42}$ cerebral spinal fluid (CSF) levels ($p<0.0001$). Follow-up comparisons showed that there were significant differences in both Tau (adjusted $p<0.0001$), and $A\beta_{1-42}$ (adjusted $p = 0.006$) following Bonferroni correction for multiple comparisons. As expected, a one-way ANOVA also showed a significant difference in normalized brain volumes between the NEC and Alzheimer disease groups ($p<0.0001$). Follow-up comparisons showed

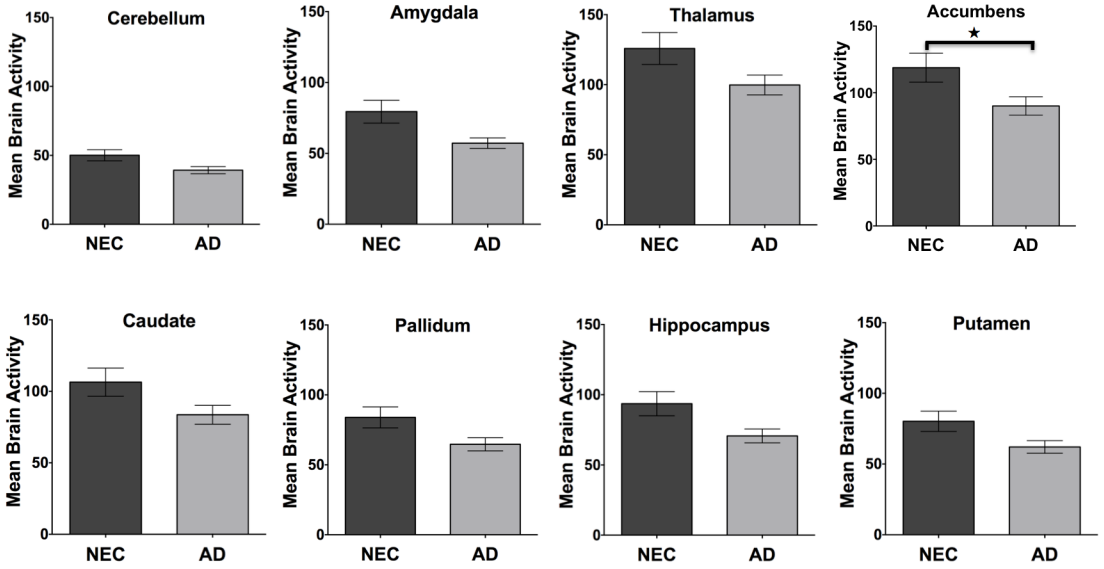


**Fig 4. Regional brain activity.** The average brain activity measured by RS-fMRI in NEC and Alzheimer disease subjects in the cerebellum, amygdala, thalamus, accumbens, caudate, pallidum, hippocampus, and putamen. The error bars represent the standard error of the mean and asterisks show significant differences between groups (adjusted *p* value, Bonferroni).

https://doi.org/10.1371/journal.pone.0178529.g004

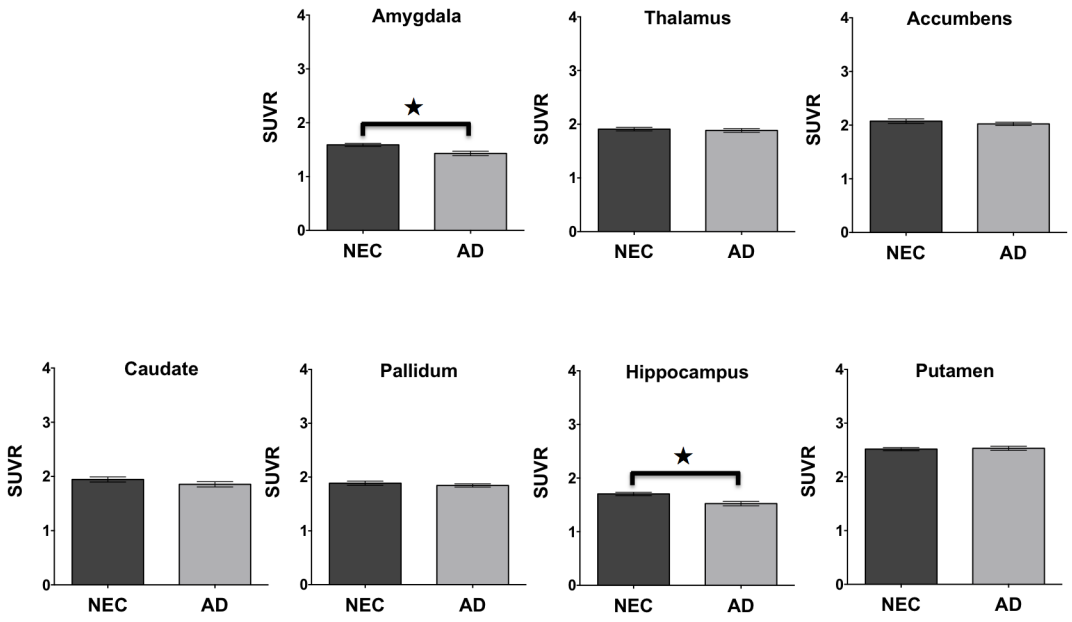


**Fig 5. Regional glucose metabolism.** The average glucose metabolism measured by FDG-PET SUVR in NEC and Alzheimer disease subjects in the amygdala, thalamus, accumbens, caudate, pallidum, hippocampus, and putamen. The error bars represent the standard error of the mean and asterisks show significant differences between groups (adjusted *p* value, Bonferroni).

https://doi.org/10.1371/journal.pone.0178529.g005

significant differences in normalized volume measured using MRI in the hippocampus ($p = 0.01$) between the two groups.

## Association between neuronal activity and glucose metabolism

A voxel by voxel correlation between gray matter RS-fMRI brain activity and the rate of glucose metabolism from the FDG-PET is shown in Fig 6 for one NEC (r = 0.81, $p<0.0001$) and

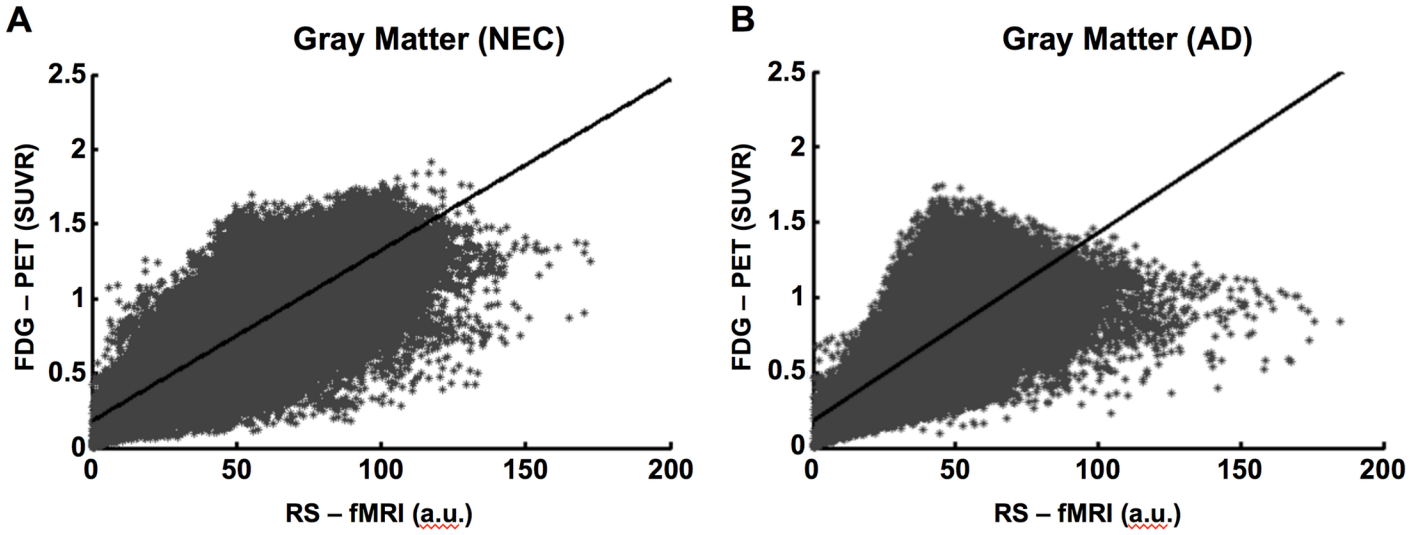


**Fig 6. Relationship between glucose metabolism using FDG-PET and brain activity measured by RS-fMRI.** Voxel by Voxel correlation of pixel intensity in gray matter (r = 0.81, $p< 0.001$) from a healthy elderly subject (A) and a patient with Alzheimer disease (B) (r = 0.77, $p< 0.001$) between brain activity using RS-fMRI and corrected glucose metabolism using FDG-PET SUVR.

https://doi.org/10.1371/journal.pone.0178529.g006

subject with Alzheimer disease (r = 0.77, $p<0.0001$). Correlations were similar in all subjects (S1 and S2 Figs). The average r-value ± SD associated with the correlation between gray matter activity measured using RS-fMRI and the rate of glucose metabolism measured using FDG-PET was 0.77 ± 0.04 for the NEC group and 0.73 ± 0.03 for the Alzheimer disease group. The average *y*-intercept ± SD for the NEC group was 0.23 ± 0.03 and for the Alzheimer disease group was 0.23 ± 0.03.

## Comparison of neuronal components in NEC and Alzheimer disease

The average ± SD of the number of neuronal components was 6.4 ± 1.5 for the NEC group and 5.0 ± 1.2 for the Alzheimer disease group. Unpaired t-test (two-tailed) showed significantly fewer neuronal components in the Alzheimer disease group compared to the NEC group ($p = 0.007$). Pooling all subjects, the average number of neuronal components was positively correlated with MMSE score (r = 0.30, $p = 0.002$) (S3 Fig). The average ± SD of the RS-fMRI neuronal activity (Eq 2) summed across all neuronal components in whole brain was 54.8 ± 18.3 in the NEC group and 40.6 ± 10.4 in the Alzheimer disease group. Unpaired t-test (two-tailed) showed significantly lower neuronal activity in the Alzheimer disease group compared to the NEC group ($p = 0.01$) (S4 Fig).

## Association between neuronal activity and cognitive function

The relationship between RS-fMRI brain activity and clinical cognitive measurement is shown for several brain regions in Fig 7 when pooling all groups. However, the correlations between

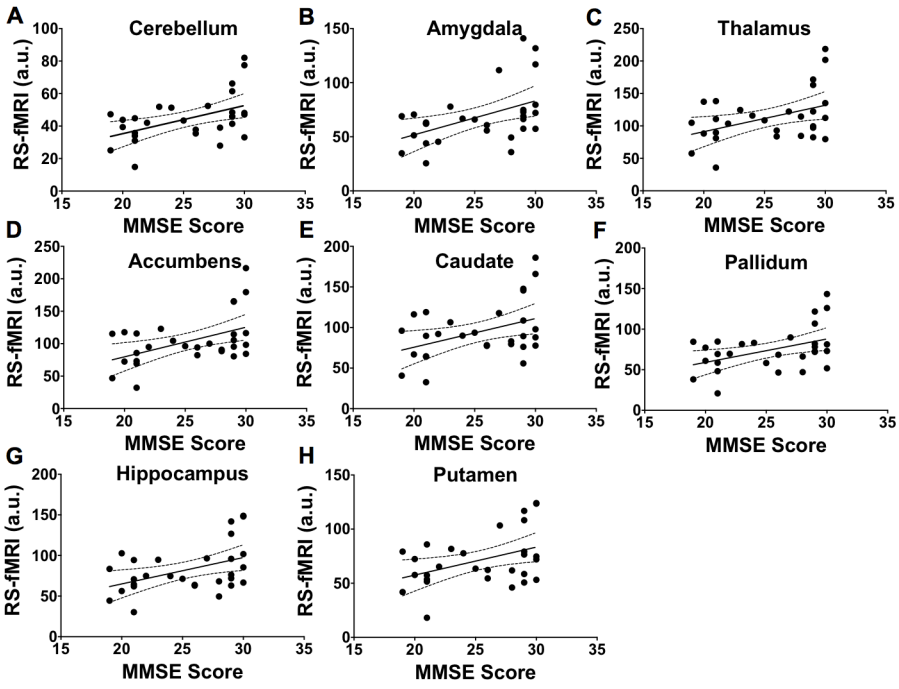


**Fig 7. Relationship between mean brain activities measured using RS-fMRI and cognition function.** The 95% confidence intervals for the regressions are shown as dotted lines. Association between MMSE score and brain activity in cerebellum (r = 0.50, $p = 0.007$, A), amygdala (r = 0.47, $p = 0.009$, B), thalamus (r = 0.42, $p = 0.02$, C), accumbens (r = 0.48, $p = 0.008$, D), caudate (r = 0.41, $p = 0.02$, E), pallidum (r = 0.44, $p = 0.01$, F), hippocampus (r = 0.44, $p = 0.01$, G), and putamen (r = 0.41, $p = 0.02$, H). These correlations were not significant following Bonferroni correction for multiple comparisons.

https://doi.org/10.1371/journal.pone.0178529.g007

the MMSE score and brain activity in the cerebellum (r = 0.50, $p = 0.007$), amygdala (r = 0.47, $p = 0.009$), thalamus (r = 0.42, $p = 0.02$), accumbens (r = 0.48, $p = 0.008$), caudate (r = 0.41, $p = 0.02$), pallidum (r = 0.44, $p = 0.01$), hippocampus (r = 0.44, $p = 0.01$), and putamen (r = 0.41, $p = 0.02$) were not significant following Bonferroni correction.

## Association between neuronal activity and amyloid beta$_{1\text{-}42}$

The relationship between RS-fMRI brain activity and $A\beta_{1-42}$ CSF level is shown for several brain regions in Fig 8 for all subjects. However, the correlations between the RS-fMRI brain activity and $A\beta_{1-42}$ in the cerebellum (r = 0.40, $p = 0.03$), amygdala (r = 0.51, $p = 0.004$), accumbens (r = 0.37, $p = 0.04$), pallidum (r = 0.41, $p = 0.02$), and putamen (r = 0.41, $p = 0.02$) were not significant following Bonferroni correction.

## Comparison of classification accuracy

The classification accuracy of subjects using brain activity measured by RS-fMRI and relative glucose metabolism rate measured using FDG-PET is provided in Table 2. The greatest classification accuracy, sensitivity, and specificity were obtained when using FDG-PET measurement from the hippocampus. The classification model that used glucose metabolism in the hippocampus measured by FDG-PET achieved 85% average accuracy, 84% sensitivity and 85% specificity (Table 2). The models that used brain activity in the hippocampus or accumbens resulted in a lower accuracy, sensitivity, and specificity (Table 2). However, the model that combined normalized hippocampal volume and neuronal activity of RS-fMRI from the hippocampus achieved 80% average accuracy, 72% sensitivity and 89% specificity, providing a similar accuracy and specificity to that observed with FDG-PET glucose metabolism in the hippocampus.

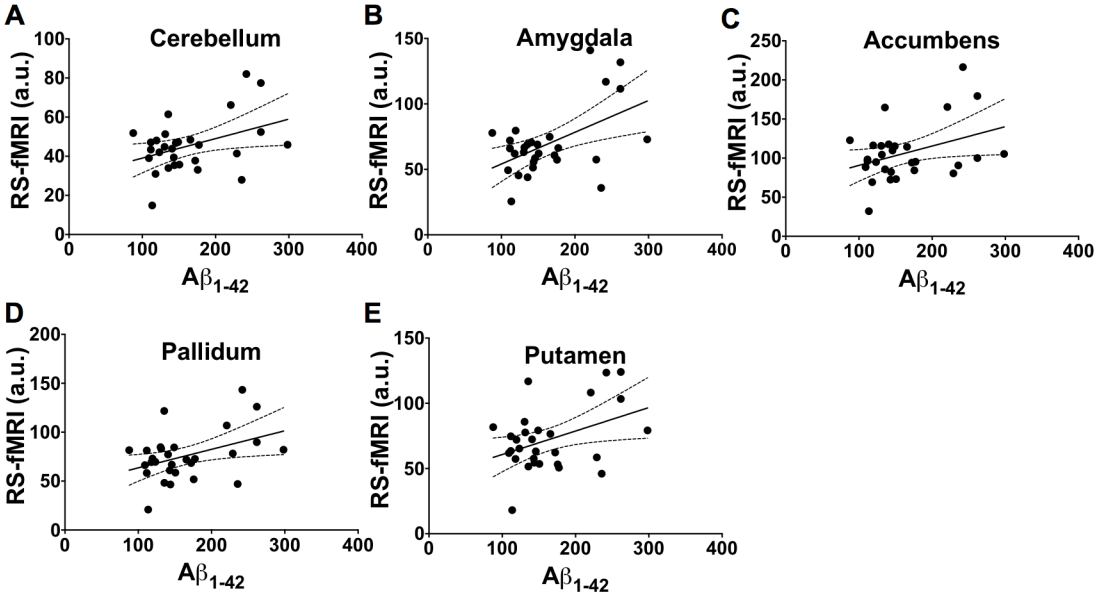


**Fig 8. Relationship between mean brain activity measured using RS-fMRI and CSF derived Amyloid Beta$_{1\text{-}42}$.** The 95% confidence intervals for the regressions are shown as dotted lines. Association between the brain activity and $A\beta_{1-42}$ in the cerebellum (r = 0.40, $p = 0.03$, A), amygdala (r = 0.51, $p = 0.004$, B), accumbens (r = 0.37, $p = 0.04$, C), pallidum (r = 0.41, $p = 0.02$, D), and putamen (r = 0.41, $p = 0.02$, E). These correlations were not significant following Bonferroni correction for multiple comparisons.

https://doi.org/10.1371/journal.pone.0178529.g008

**Table 2. Classification results for RS-fMRI brain activity, glucose metabolism measured by FDG-PET SUVR, and normalized volume measured using MRI.** The 95% confidence interval (CI) is provided in parentheses.

| SVM_linear (leave-one-out-test) | Accuracy | Sensitivity | Specificity |
|---|---|---|---|
| RS-fMRI (Hippocampus) | 0.75 | 0.70 | 0.78 |
| | | (0.68–0.75) | (0.70–0.82) |
| RS-fMRI (Accumbens) | 0.56 | 0.42 | 0.68 |
| | | (0.42–0.57) | (0.58–0.70) |
| RS-fMRI (Hippocampus, and Amygdala) | 0.65 | 0.57 | 0.71 |
| | | (0.40–0.60) | (0.69–0.80) |
| FDG-PET (Hippocampus) | 0.85 | 0.84 | 0.85 |
| | | (0.77–0.85) | (0.75–0.85) |
| FDG-PET (Hippocampus, and Amygdala) | 0.76 | 0.84 | 0.68 |
| | | (0.78–0.84) | (0.62–0.75) |
| MRI (Hippocampus) | 0.67 | 0.64 | 0.70 |
| | | (0.60–0.68) | (0.68–0.74) |
| RS-fMRI (Accumbens) + MRI (Hippocampus) | 0.70 | 0.63 | 0.73 |
| | | (0.60–0.75) | (0.73–0.80) |
| RS-fMRI (Hippocampus) + MRI (Hippocampus) | 0.80 | 0.72 | 0.89 |
| | | (0.65–0.76) | (0.83–0.90) |

SVM = support vector machine, FDG-PET = $^{18}$fludeoxyglucose-PET, RS-fMRI = resting state functional MRI.

https://doi.org/10.1371/journal.pone.0178529.t002

## Discussion

In this study we define a new metric related to neuronal activity based on the square root of the temporal standard deviation of the RS-fMRI signal summed across all *neuronal components* within a pixel. As a proof of principle, this new RS-fMRI based metric was used to compare brain activity in normal elderly subjects and patients with mild Alzheimer disease. The brain activity measurement is dependent on both the number of neuronal components and the temporal fluctuation associated with each component. Overall lower brain activity was observed in the mild Alzheimer disease group, particularly within the accumbens. A similar comparison in the same subjects using FDG-PET also showed overall group differences indicating lower glucose metabolism in the amygdala, and hippocampus. In a pixel-by-pixel analysis, brain activity derived from RS-fMRI was found to be strongly correlated with glucose metabolism measured by FDG-PET in gray matter.

The FDG-PET results from the current study are consistent with previous FDG-PET studies that have shown reduced glucose metabolism in subjects with Alzheimer disease [28, 45]. Reduced glucose metabolism has also been observed in the posterior cingulate, temporal, parietal lobes and later the frontal lobe [28, 46]. Mosconi *et. al.* [47] showed that glucose metabolism in the hippocampus and the entorhinal cortex is also reduced in the preclinical stage of Alzheimer disease. In addition, Jagust *et. al.* [48] has demonstrated that medial temporal and parietal glucose metabolism predicts cognitive decline. Glucose consumption measured by FDG-PET is also linearly associated with neuronal activity [49]. Therefore glucose consumption is considered an important indicator of presymptomatic Alzheimer disease [50].

A few RS-fMRI studies have also examined functional *network* activity in healthy subjects compared to people with Alzheimer disease. Seed based analyses [17, 18] have shown decreased functional connectivity (FC) in the medial temporal cortex, prefrontal cortex, precuneus, posterior cingulate, hippocampus, and thalamus in people with Alzheimer disease. Similar studies using ICA methods demonstrated reduced FC in precuneus, posterior cingulate,

and parietal lobe in people with amnestic mild cognitive impairment (aMCI) [51] while Zhou *et. al.* [52] showed decreased FC in the default mode network including the hippocampus and the medial temporal lobe in people with Alzheimer disease. In the current study we did *not* examine functional connectivity, but instead used the RS-fMRI neuronal signal fluctuation to define a new indicator of brain activity. When examining activity in specific brain regions, the newly defined measurement of neuronal activity showed trends toward correlation with the MMSE score and $A\beta_{1-42}$, but these associations did not remain significant following Bonferroni correction.

The new RS-fMRI metric related to brain activity showed regional differences between NEC and Alzheimer disease subjects that were different than those observed with FDG-PET. Previous studies have found that cerebral blood flow is closely coupled with brain metabolism [53, 54], and that both are decreased in people with Alzheimer's disease [55–59]. Previous studies have also shown that there is an association between the resting brain activity and resting brain metabolism [60]. The strong correlation observed between RS-fMRI measured gray matter activity and FDG-PET measured glucose consumption in the current study is consistent with the notion that glucose metabolism is tightly coupled to the RS-fMRI measured brain activity. This result is also consistent with a recent study by Aiello *et. al.* [61] who showed a voxel-wise relationship between functional connectivity maps from RS-fMRI and glucose uptake measured by simultaneous FDG-PET in healthy subjects. Another recent study by Nugent *et. al.* [62] demonstrated that the correlation between functional connectivity maps derived from RS-fMRI and glucose metabolism measured by FDG-PET was lower in temporal lobe epilepsy patients compared to control subjects.

The group differentiation accuracy achieved using the brain activity metric in the accumbens measured by RS-fMRI was lower than that found when using FDG-PET measured glucose metabolism in the hippocampus (0.85). However, when combining hippocampal volume with brain activity from RS-fMRI in the hippocampus, the classification accuracy increased to 0.80, which is comparable to the FDG-PET results and significantly greater than using hippocampal volume alone. The specificity achieved when using the combined MRI-based measurements (0.89) was also greater than that achieved by FDG-PET and hippocampal volume alone. These results suggest that the combination of these MRI-based features could help to discriminate between a group of healthy elderly subjects and people with AD.

This proof of concept study demonstrates that decreased resting-state brain activity is associated with decreased brain glucose metabolism in mild Alzheimer disease. Furthermore, we demonstrated group classification based on a first-order textural feature (standard deviation) of the RS-fMRI neuronal signal. There are several limitations of the current study that should be considered. First, the sample size was limited by the availability of subjects with both ten-minute RS-fMRI data and FDG-PET. Regardless, the new metric was still able to differentiate between NEC and mild Alzheimer disease groups. Another limitation of this study is that we did not perform gray atrophy correction for either the RS-fMRI or FDG-PET signal changes. Therefore gray matter volume reduction in the hippocampus may partly explain the reduced RS-fMRI and FDG-PET measured brain activity. However, Mosconi *et. al.* [63] showed FDG-PET measured hypometabolism in the hippocampus despite atrophy correction in hippocampus. Gray matter atrophy measurements in the current study did show significant differences in the hippocampus between the two groups. However a classification model that included both the hippocampal volume and RS-fMRI brain activity showed an improved result to classification using either metric alone. Therefore, including this straightforward measurement of neuronal activity by RS-fMRI with existing markers of neurodegeneration may increase the reliability of detecting Alzheimer's disease. Future studies will evaluate the

potential to identify people with mild cognitive impairment that progress to AD and whether this metric shows improvement following treatment.

## Supporting information

**S1 Fig. The association between RS-fMRI and FDG-PET SUVR in the healthy elderly group.** The scatter plots represent the voxel by voxel correlation of pixel intensity in the gray matter of healthy elderly subjects between brain activity using RS-fMRI and corrected glucose metabolism using FDG-PET SUVR. Each graph represents the results from a different individual.
(TIF)

**S2 Fig. The association between RS-fMRI and FDG-PET SUVR in the Alzheimer disease group.** The scatter plots represent the voxel by voxel correlation of pixel intensity in the gray matter of Alzheimer disease subjects between brain activity using RS-fMRI and corrected glucose metabolism using FDG-PET SUVR. Each graph represents the results from a different individual.
(TIF)

**S3 Fig. The relationship between the number of neuronal components and cognition function measured by the MMSE score.** The 95% confidence intervals for the regressions are shown as dotted lines. A significant correlation was found between MMSE score and the number of neuronal components ($r = 0.30$, $p = 0.002$).
(TIF)

**S4 Fig. Component specific brain activity maps in one healthy elderly subject and one subject with Alzheimer disease.** Each image represents the square root of the standard deviation of the magnitude of the BOLD signal fluctuation. In this example, data from each identified neuronal component is provided in a different row. Eight neuronal components were identified in the healthy subject while only six neuronal components were identified in the subject with AD.
(TIF)

**S1 Table. Healthy elderly control subjects.**
(DOCX)

**S2 Table. People with Alzheimer's disease.**
(DOCX)

## Acknowledgments

Data used in preparation of this article were obtained from the Alzheimer's Disease Neuroimaging Initiative (ADNI) database (adni.loni.ucla.edu). As such, the investigators within the ADNI contributed to the design and implementation of ADNI and/or provided data but did not participate in analysis or writing of this report.

### Contributors

A complete listing of ADNI investigators can be found at: https://adni.loni.usc.edu/wp-content/uploads/how_to_apply/ADNI_Acknowledgement_List.pdf.

## Author Contributions

**Conceptualization:** RB RSM MJB SK.

**Data curation:** RB AS SK.

**Formal analysis:** RB RSM KM AS SK.

**Funding acquisition:** RB MJB NR.

**Investigation:** SK.

**Methodology:** RB RSM AS NR SK.

**Project administration:** RB SK.

**Resources:** RB MJB AS.

**Software:** AS FAG SK.

**Supervision:** RB.

**Validation:** RB RSM MJB AS FAG KM SK.

**Visualization:** RB RSM MJB AS KM NR SK.

**Writing – original draft:** RB SK.

**Writing – review & editing:** RB RSM MJB AS FAG KM NR SK.

## References


1. Terry RD, Masliah E, Salmon DP, Butters N, DeTeresa R, Hill R, et al. Physical basis of cognitive alterations in Alzheimer's disease: synapse loss is the major correlate of cognitive impairment. Annals of neurology. 1991; 30(4):572–80. Epub 1991/10/01. https://doi.org/10.1002/ana.410300410 PMID: 1789684.
2. Nestor PJ, Scheltens P, Hodges JR. Advances in the early detection of Alzheimer's disease. Nat Med. 2004; 10 Suppl:S34–41. Epub 2004/08/10. https://doi.org/10.1038/nrn1433 PMID: 15298007.
3. Reddy PH, Beal MF. Amyloid beta, mitochondrial dysfunction and synaptic damage: implications for cognitive decline in aging and Alzheimer's disease. Trends in molecular medicine. 2008; 14(2):45–53. https://doi.org/10.1016/j.molmed.2007.12.002 PMID: 18218341;
4. Jack CR Jr., Slomkowski M, Gracon S, Hoover TM, Felmlee JP, Stewart K, et al. MRI as a biomarker of disease progression in a therapeutic trial of milameline for AD. Neurology. 2003; 60(2):253–60. PMID: 12552040.
5. Kazemifar S, Drozd JJ, Rajakumar N, Borrie MJ, Bartha R, Alzheimer's Disease Neuroimaging I. Automated algorithm to measure changes in medial temporal lobe volume in Alzheimer disease. J Neurosci Methods. 2014; 227:35–46. https://doi.org/10.1016/j.jneumeth.2014.01.033 PMID: 24518149.
6. Scheltens P, Fox N, Barkhof F, De Carli C. Structural magnetic resonance imaging in the practical assessment of dementia: beyond exclusion. Lancet neurology. 2002; 1(1):13–21. PMID: 12849541.
7. Iacoboni M, Baron JC, Frackowiak RS, Mazziotta JC, Lenzi GL. Emission tomography contribution to clinical neurology. Clinical neurophysiology: official journal of the International Federation of Clinical Neurophysiology. 1999; 110(1):2–23. PMID: 10348316.
8. Cunnane S, Nugent S, Roy M, Courchesne-Loyer A, Croteau E, Tremblay S, et al. Brain fuel metabolism, aging, and Alzheimer's disease. Nutrition. 2011; 27(1):3–20. https://doi.org/10.1016/j.nut.2010.07.021 PMID: 21035308;
9. Alexander GE, Chen K, Pietrini P, Rapoport SI, Reiman EM. Longitudinal PET Evaluation of Cerebral Metabolic Decline in Dementia: A Potential Outcome Measure in Alzheimer's Disease Treatment Studies. The American journal of psychiatry. 2002; 159(5):738–45. PMID: 11986126. https://doi.org/10.1176/appi.ajp.159.5.738
10. Fox MD, Raichle ME. Spontaneous fluctuations in brain activity observed with functional magnetic resonance imaging. Nature reviews. 2007; 8(9):700–11. Epub 2007/08/21. nrn2201 [pii] https://doi.org/10.1038/nrn2201 PMID: 17704812.

11. Biswal B, Yetkin FZ, Haughton VM, Hyde JS. Functional connectivity in the motor cortex of resting human brain using echo-planar MRI. Magn Reson Med. 1995; 34(4):537–41. Epub 1995/10/01. PMID: 8524021.
12. Smith SM, Fox PT, Miller KL, Glahn DC, Fox PM, Mackay CE, et al. Correspondence of the brain's functional architecture during activation and rest. P Natl Acad Sci USA. 2009; 106(31):13040–5. https://doi.org/10.1073/Pnas.0905267106 PMID: 19620724
13. Greicius MD, Srivastava G, Reiss AL, Menon V. Default-mode network activity distinguishes Alzheimer's disease from healthy aging: evidence from functional MRI. Proc Natl Acad Sci U S A. 2004; 101 (13):4637–42. Epub 2004/04/09. https://doi.org/10.1073/pnas.0308627101 PMID: 15070770;
14. Wang L, Zang Y, He Y, Liang M, Zhang X, Tian L, et al. Changes in hippocampal connectivity in the early stages of Alzheimer's disease: evidence from resting state fMRI. NeuroImage. 2006; 31(2):496–504. Epub 2006/02/14. https://doi.org/10.1016/j.neuroimage.2005.12.033 PMID: 16473024.
15. Allen G, Barnard H, McColl R, Hester AL, Fields JA, Weiner MF, et al. Reduced hippocampal functional connectivity in Alzheimer disease. Arch Neurol. 2007; 64(10):1482–7. Epub 2007/10/10. 64/10/1482 [pii] https://doi.org/10.1001/archneur.64.10.1482 PMID: 17923631.
16. Chen G, Ward BD, Xie C, Li W, Wu Z, Jones JL, et al. Classification of Alzheimer disease, mild cognitive impairment, and normal cognitive status with large-scale network analysis based on resting-state functional MR imaging. Radiology. 2011; 259(1):213–21. https://doi.org/10.1148/radiol.10100734 PMID: 21248238;
17. Wang K, Liang M, Wang L, Tian L, Zhang X, Li K, et al. Altered functional connectivity in early Alzheimer's disease: a resting-state fMRI study. Hum Brain Mapp. 2007; 28(10):967–78. Epub 2006/11/30. https://doi.org/10.1002/hbm.20324 PMID: 17133390.
18. Zhang HY, Wang SJ, Xing J, Liu B, Ma ZL, Yang M, et al. Detection of PCC functional connectivity characteristics in resting-state fMRI in mild Alzheimer's disease. Behav Brain Res. 2009; 197(1):103–8. Epub 2008/09/13. S0166-4328(08)00435-X [pii] https://doi.org/10.1016/j.bbr.2008.08.012 PMID: 18786570.
19. Fox MD, Snyder AZ, Vincent JL, Corbetta M, Van Essen DC, Raichle ME. The human brain is intrinsically organized into dynamic, anticorrelated functional networks. P Natl Acad Sci USA. 2005; 102 (27):9673–8. https://doi.org/10.1073/Pnas.0504136102 PMID: 15976020
20. Bell AJ, Sejnowski TJ. An information-maximization approach to blind separation and blind deconvolution. Neural computation. 1995; 7(6):1129–59. Epub 1995/11/01. PMID: 7584893.
21. Beckmann CF, DeLuca M, Devlin JT, Smith SM. Investigations into resting-state connectivity using independent component analysis. Philos T Roy Soc B. 2005; 360(1457):1001–13. https://doi.org/10.1098/Rstb.2005.1634 PMID: 16087444
22. Damoiseaux JS, Rombouts SA, Barkhof F, Scheltens P, Stam CJ, Smith SM, et al. Consistent resting-state networks across healthy subjects. Proc Natl Acad Sci U S A. 2006; 103(37):13848–53. Epub 2006/09/02. 0601417103 [pii] https://doi.org/10.1073/pnas.0601417103 PMID: 16945915;
23. McKeown MJ, Makeig S, Brown GG, Jung TP, Kindermann SS, Bell AJ, et al. Analysis of fMRI data by blind separation into independent spatial components. Hum Brain Mapp. 1998; 6(3):160–88. Epub 1998/07/23. PMID: 9673671.
24. Thomas CG, Harshman RA, Menon RS. Noise reduction in BOLD-based fMRI using component analysis. NeuroImage. 2002; 17(3):1521–37. https://doi.org/10.1006/nimg.2002.1200 PMID: 12414291
25. Demertzi A, Gomez F, Crone JS, Vanhaudenhuyse A, Tshibanda L, Noirhomme Q, et al. Multiple fMRI system-level baseline connectivity is disrupted in patients with consciousness alterations. Cortex; a journal devoted to the study of the nervous system and behavior. 2014; 52:35–46. Epub 2014/02/01. https://doi.org/10.1016/j.cortex.2013.11.005 PMID: 24480455.
26. Agosta F, Pievani M, Geroldi C, Copetti M, Frisoni GB, Filippi M. Resting state fMRI in Alzheimer's disease: beyond the default mode network. Neurobiology of aging. 2012; 33(8):1564–78. https://doi.org/10.1016/j.neurobiolaging.2011.06.007 PMID: 21813210.
27. Minoshima S, Giordani B, Berent S, Frey KA, Foster NL, Kuhl DE. Metabolic reduction in the posterior cingulate cortex in very early Alzheimer's disease. Annals of neurology. 1997; 42(1):85–94. https://doi.org/10.1002/ana.410420114 PMID: 9225689
28. Nestor PJ, Fryer TD, Smielewski P, Hodges JR. Limbic hypometabolism in Alzheimer's disease and mild cognitive impairment. Annals of neurology. 2003; 54(3):343–51. https://doi.org/10.1002/ana.10669 PMID: 12953266.
29. Mosconi L. Brain glucose metabolism in the early and specific diagnosis of Alzheimer's disease. FDG-PET studies in MCI and AD. European journal of nuclear medicine and molecular imaging. 2005; 32 (4):486–510. https://doi.org/10.1007/s00259-005-1762-7 PMID: 15747152.

30. Sheline YI, Raichle ME, Snyder AZ, Morris JC, Head D, Wang S, et al. Amyloid plaques disrupt resting state default mode network connectivity in cognitively normal elderly. Biological psychiatry. 2010; 67 (6):584–7. https://doi.org/10.1016/j.biopsych.2009.08.024 PMID: 19833321;

31. Mormino EC, Smiljic A, Hayenga AO, Onami SH, Greicius MD, Rabinovici GD, et al. Relationships between Beta-Amyloid and Functional Connectivity in Different Components of the Default Mode Network in Aging. Cerebral Cortex. 2011; 21(10):2399–407. https://doi.org/10.1093/cercor/bhr025 PMID: 21383234

32. Di X, Biswal BB, Alzheimer's Disease Neuroimaging I. Metabolic brain covariant networks as revealed by FDG-PET with reference to resting-state fMRI networks. Brain connectivity. 2012; 2(5):275–83. https://doi.org/10.1089/brain.2012.0086 PMID: 23025619;

33. Tomasi D, Wang GJ, Volkow ND. Energetic cost of brain functional connectivity. Proc Natl Acad Sci U S A. 2013; 110(33):13642–7. https://doi.org/10.1073/pnas.1303346110 PMID: 23898179;

34. Riedl V, Bienkowska K, Strobel C, Tahmasian M, Grimmer T, Forster S, et al. Local activity determines functional connectivity in the resting human brain: a simultaneous FDG-PET/fMRI study. The Journal of neuroscience: the official journal of the Society for Neuroscience. 2014; 34(18):6260–6. https://doi.org/10.1523/JNEUROSCI.0492-14.2014 PMID: 24790196.

35. Barkhof F, Haller S, Rombouts SA. Resting-state functional MR imaging: a new window to the brain. Radiology. 2014; 272(1):29–49. https://doi.org/10.1148/radiol.14132388 PMID: 24956047.

36. Jack CR Jr., Bernstein MA, Fox NC, Thompson P, Alexander G, Harvey D, et al. The Alzheimer's Disease Neuroimaging Initiative (ADNI): MRI methods. J Magn Reson Imaging. 2008; 27(4):685–91. Epub 2008/02/28. https://doi.org/10.1002/jmri.21049 PMID: 18302232;

37. Wyman BT, Harvey DJ, Crawford K, Bemstein MA, Carmichael O, Cole PE, et al. Standardization of analysis sets for reporting results from ADNI MRI data. Alzheimers & Dementia. 2013; 9(3):332–7. https://doi.org/10.1016/J.Jalz.2012.06.004 PMID: 23110865

38. Jagust WJ, Bandy D, Chen K, Foster NL, Landau SM, Mathis CA, et al. The Alzheimer's Disease Neuroimaging Initiative positron emission tomography core. Alzheimer's & dementia: the journal of the Alzheimer's Association. 2010; 6(3):221–9. Epub 2010/05/11. https://doi.org/10.1016/j.jalz.2010.03.003 PMID: 20451870;

39. Folstein MF, Folstein SE, McHugh PR. "Mini-mental state". A practical method for grading the cognitive state of patients for the clinician. J Psychiatr Res. 1975; 12(3):189–98. PMID: 1202204.

40. Calhoun VD, Adali T, Pearlson GD, Pekar JJ. A method for making group inferences from functional MRI data using independent component analysis. Hum Brain Mapp. 2001; 14(3):140–51. Epub 2001/09/18. PMID: 11559959.

41. Patenaude B, Smith SM, Kennedy DN, Jenkinson M. A Bayesian model of shape and appearance for subcortical brain segmentation. NeuroImage. 2011; 56(3):907–22. https://doi.org/10.1016/j.neuroimage.2011.02.046 PMID: 21352927;

42. Shidahara M, Tsoumpas C, Hammers A, Boussion N, Visvikis D, Suhara T, et al. Functional and structural synergy for resolution recovery and partial volume correction in brain PET. NeuroImage. 2009; 44 (2):340–8. https://doi.org/10.1016/j.neuroimage.2008.09.012 PMID: 18852055.

43. Dukart J, Kherif F, Mueller K, Adaszewski S, Schroeter ML, Frackowiak RS, et al. Generative FDG-PET and MRI model of aging and disease progression in Alzheimer's disease. PLoS computational biology. 2013; 9(4):e1002987. Epub 2013/04/18. https://doi.org/10.1371/journal.pcbi.1002987 PMID: 23592957;

44. Cortes C, Vapnik V. Support-Vector Networks. Mach Learn. 1995; 20(3):273–97. https://doi.org/10.1023/A:1022627411411

45. Mosconi L, De Santi S, Li J, Tsui WH, Li Y, Boppana M, et al. Hippocampal hypometabolism predicts cognitive decline from normal aging. Neurobiology of aging. 2008; 29(5):676–92. https://doi.org/10.1016/j.neurobiolaging.2006.12.008 PMID: 17222480;

46. Del Sole A, Clerici F, Chiti A, Lecchi M, Mariani C, Maggiore L, et al. Individual cerebral metabolic deficits in Alzheimer's disease and amnestic mild cognitive impairment: an FDG PET study. European journal of nuclear medicine and molecular imaging. 2008; 35(7):1357–66. https://doi.org/10.1007/s00259-008-0773-6 PMID: 18418593.

47. Mosconi L, Pupi A, De Leon MJ. Brain glucose hypometabolism and oxidative stress in preclinical Alzheimer's disease. Annals of the New York Academy of Sciences. 2008; 1147:180–95. https://doi.org/10.1196/annals.1427.007 PMID: 19076441;

48. Jagust W, Gitcho A, Sun F, Kuczynski B, Mungas D, Haan M. Brain imaging evidence of preclinical Alzheimer's disease in normal aging. Annals of neurology. 2006; 59(4):673–81. https://doi.org/10.1002/ana.20799 PMID: 16470518.

49. Mosconi L. Glucose metabolism in normal aging and Alzheimer's disease: Methodological and physiological considerations for PET studies. Clinical and translational imaging. 2013; 1(4). https://doi.org/10.1007/s40336-013-0026-y PMID: 24409422;

50. Nordberg A, Rinne JO, Kadir A, Langstrom B. The use of PET in Alzheimer disease. Nature reviews Neurology. 2010; 6(2):78–87. Epub 2010/02/09. https://doi.org/10.1038/nrneurol.2009.217 PMID: 20139997.

51. Qi Z, Wu X, Wang Z, Zhang N, Dong H, Yao L, et al. Impairment and compensation coexist in amnestic MCI default mode network. NeuroImage. 2010; 50(1):48–55. https://doi.org/10.1016/j.neuroimage.2009.12.025 PMID: 20006713.

52. Zhou J, Greicius MD, Gennatas ED, Growdon ME, Jang JY, Rabinovici GD, et al. Divergent network connectivity changes in behavioural variant frontotemporal dementia and Alzheimer's disease. Brain: a journal of neurology. 2010; 133(Pt 5):1352–67. https://doi.org/10.1093/brain/awq075 PMID: 20410145;

53. Solhi H, Ghahremani R, Kazemifar AM, Hoseini Yazdi Z. Silymarin in treatment of non-alcoholic steatohepatitis: A randomized clinical trial. Caspian journal of internal medicine. 2014; 5(1):9–12. PMID: 24490006;

54. Raichle ME, Grubb RL, Gado MH, Eichling JO, Terpogossian MM. Correlation between Regional Cerebral Blood-Flow and Oxidative-Metabolism. Archives of neurology. 1976; 33(8):523–6. PMID: 942309

55. Alavi A, Ferris S, Wolf A, Reivich M, Farkas T, Dann R, et al. Determination of Cerebral Metabolism in Senile Dementia Using Deoxyglucose-F-18 and Positron Emission Tomography. Journal of Nuclear Medicine. 1980; 21(6):P21–P.

56. Frackowiak RS, Pozzilli C, Legg NJ, Du Boulay GH, Marshall J, Lenzi GL, et al. Regional cerebral oxygen supply and utilization in dementia. A clinical and physiological study with oxygen-15 and positron tomography. Brain: a journal of neurology. 1981; 104(Pt 4):753–78. PMID: 6976816.

57. Gottschalk A, Hoffer PB. Positron emission tomography in aging and dementia: effect of cerebral atrophy. Investigative radiology. 1988; 23(11):879–80. PMID: 3264826.

58. Matsuda H. Cerebral blood flow and metabolic abnormalities in Alzheimer's disease. Annals of nuclear medicine. 2001; 15(2):85–92. PMID: 11448080.

59. Niwa K, Kazama K, Younkin SG, Carlson GA, Iadecola C. Alterations in cerebral blood flow and glucose utilization in mice overexpressing the amyloid precursor protein. Neurobiology of disease. 2002; 9(1):61–8. https://doi.org/10.1006/nbdi.2001.0460 PMID: 11848685.

60. Li ZJ, Zhu YS, Childress AR, Detre JA, Wang Z. Relations between BOLD fMRI-Derived Resting Brain Activity and Cerebral Blood Flow. Plos One. 2012; 7(9). ARTN e44556 https://doi.org/10.1371/journal.pone.0044556 PMID: 23028560

61. Aiello M, Salvatore E, Cachia A, Pappata S, Cavaliere C, Prinster A, et al. Relationship between simultaneously acquired resting-state regional cerebral glucose metabolism and functional MRI: A PET/MR hybrid scanner study. NeuroImage. 2015; 113:111–21. https://doi.org/10.1016/j.neuroimage.2015.03.017 PMID: 25791784

62. Nugent AC, Martinez A, D'Alfonso A, Zarate CA, Theodore WH. The relationship between glucose metabolism, resting-state fMRI BOLD signal, and GABA(A)-binding potential: a preliminary study in healthy subjects and those with temporal lobe epilepsy. J Cerebr Blood F Met. 2015; 35(4):583–91. https://doi.org/10.1038/jcbfm.2014.228 PMID: 25564232

63. Mosconi L, Tsui WH, De Santi S, Li J, Rusinek H, Convit A, et al. Reduced hippocampal metabolism in MCI and AD: automated FDG-PET image analysis. Neurology. 2005; 64(11):1860–7. PMID: 15955934. https://doi.org/10.1212/01.WNL.0000163856.13524.08